SbD-based Synthesis of Spline-Contoured Ogive Radome

M. Salucci, G. Oliveri, M. A. Hannan and A. Massa

Contents

1 Optimization with PSO+Kriging (no update during optimization)

1.0.1 Parameters

Optimization targets

- Number of variables: $K = 5$;
- Frequency range:
  - Minimum frequency: $f_{min} = 10.75$ $[GHz]$;
  - Maximum frequency: $f_{max} = 14.5$ $[GHz]$;
  - Number of frequency steps: $N_f = 10$ ($\Delta f \simeq 0.42$ $[GHz]$);
  - Central frequency: $f_0 = \frac{f_{min}+f_{max}}{2} \simeq 12.63$ $[GHz]$;
  - Free-space wavelength at the central frequency: $\lambda_0 = \frac{c}{f_0} = 2.38 \times 10^{-2}$ $[m]$;
- Scanning angle range:
  - Minimum scanning angle: $\theta_{min} = 0$ $[deg]$;
  - Maximum scanning angle: $\theta_{max} = 45$ $[deg]$;
  - Number of angular steps: $N_\theta = 4$ ($\theta_1 = 0$ $[deg]$, $\theta_2 = 15$ $[deg]$, $\theta_3 = 30$ $[deg]$, $\theta_4 = 45$ $[deg]$);

PSO **parameters**

- Population dimension: $P = 10$;
- Maximum number of iterations: $I_{max} = 200$;
- Fitness threshold: $\Phi^{th} = 10^{-20}$;
- Inertial weight: $w = 0.4$;
- Constant inertial velocity;
- Exploration coefficient: $c_1 = 2$;
- Exploitation coefficient: $c_2 = 2$;
- Random seed $S = 1, 2, ..., 10$;

Kriging (Gaussian Process Regressor) parameters

- Regression model: constant (Ordinary Kriging);
- Correlation models:
  - Exponential ($p = 1$);

- Initial guess for hyper-parameters θ_h: $\theta_{h,0} = 0.5$, for $h = 1, ..., K$;
- Lower bound for hyper-parameters θ_h: $min\{\theta_h\} = 0.1$, for $h = 1, ..., K$;
- Upper bound for hyper-parameters θ_h: $max\{\theta_h\} = 20.0$, for $h = 1, ..., K$;

Not-optimized (static) radome parameter

Parameter	Description	Value
L	Length of the radome	1.59×10^{-1} $[m] \simeq 6.69$ λ_0
D	Base diameter of the radome	1.27×10^{-1} $[m] \simeq 5.35$ λ_0
t_0	Thickness of the base and of the top of the radome	$8.20 \times 10^{-3}[m] \simeq \frac{\lambda_r}{2}$
z_1	z-coordinate of the spline control point 1	$\frac{L-t_0}{6}$
z_2	z-coordinate of the spline control point 2	$2\frac{L-t_0}{6}$
z_3	z-coordinate of the spline control point 3	$3\frac{L-t_0}{6}$
z_4	z-coordinate of the spline control point 4	$4\frac{L-t_0}{6}$
z_5	z-coordinate of the spline control point 5	$5\frac{L-t_0}{6}$
ν	External curvature of the radome ($\nu \in [1, 2]$)	1.449 (tangent ogive)
ε_r	Permittivity of the radome material	2.10 (Teflon)
$\tan\delta_r$	Tangent delta of the radome material	$tan\delta = 3.00 \times 10^{-4}$ @ 10.0 $[GHz]$ (Teflon)
λ_r	Wavelength in the radome material	$\lambda_r \simeq \frac{c}{f_0\sqrt{\varepsilon}} \simeq 1.64 \times 10^{-1}$

Table I: List of non-optimized radome parameters.

Antenna Parameters

- Linear dipole array placed over circular ground plane (PEC)
- Number of array elements: $N_e = 8$
- Dipole length: $l_e = \frac{\lambda_0}{2}$
- Array elements spacing: $d_e = \lambda/2$
- Spacing between the array and the ground plane: $h_e = \frac{\lambda_0}{4}$

Parameters boundaries

Parameter	Description	Min	Max
t_1	Radome thickness at the quota $z = z_1$	$6.55 \times 10^{-3}[m]$ $(0.4\lambda_r)$	$9.83 \times 10^{-3}[m]$ $(0.6\lambda_r)$
t_2	Radome thickness at the quota $z = z_2$	$6.55 \times 10^{-3}[m]$ $(0.4\lambda_r)$	$9.83 \times 10^{-3}[m]$ $(0.6\lambda_r)$
t_3	Radome thickness at the quota $z = z_3$	$6.55 \times 10^{-3}[m]$ $(0.4\lambda_r)$	$9.83 \times 10^{-3}[m]$ $(0.6\lambda_r)$
t_4	Radome thickness at the quota $z = z_4$	$6.55 \times 10^{-3}[m]$ $(0.4\lambda_r)$	$9.83 \times 10^{-3}[m]$ $(0.6\lambda_r)$
t_5	Radome thickness at the quota $z = z_5$	$6.55 \times 10^{-3}[m]$ $(0.4\lambda_r)$	$9.83 \times 10^{-3}[m]$ $(0.6\lambda_r)$

Table II: List of all considered boundaries for the optimized radome descriptors.

1.0.2 Results of the optimization (seed 1,...,10)

- Number of performed PSO iterations: $I_{tot} = I = 200$ for every seed.
- Total number of simulations: $E = \tau = 250$ (only for training).
- Final value of the fitness (predicted and actual):

	Predicted			Actual	
Seed	$\widehat{\Phi}^{init}$	$\widehat{\Phi}^{opt}$	$\frac{\widehat{\Phi}^{opt}}{\widehat{\Phi}^{init}}$	Φ^{opt}	$100\frac{\Phi^{opt}_{train}-\Phi^{opt}}{\Phi^{opt}_{train}}$
1	2.66	1.32	4.96×10^{-1}	1.47	3.37
2	1.96	1.33	6.79×10^{-1}	1.55	-1.45
3	1.99	1.36	6.83×10^{-1}	1.51	1.26
4	2.10	1.32	6.29×10^{-1}	1.47	3.48
5	1.83	1.32	7.21×10^{-1}	1.48	2.88
6	1.89	1.32	6.98×10^{-1}	1.48	2.88
7	2.23	1.32	5.92×10^{-1}	1.48	2.88
8	2.67	1.32	4.94×10^{-1}	1.48	2.81
9	2.22	1.32	5.95×10^{-1}	1.48	2.87
10	2.68	1.32	4.93×10^{-1}	1.48	2.88

Table III: Final value of the predicted and actual fitness values ($\widehat{\Phi}^{init}$ is the initial predicted fitness, $\widehat{\Phi}^{opt}$ is the optimal predicted fitness, Φ^{opt} is the optimal actual fitness and $\Phi^{opt}_{train} = 1.53$ is the best individual in the training set).

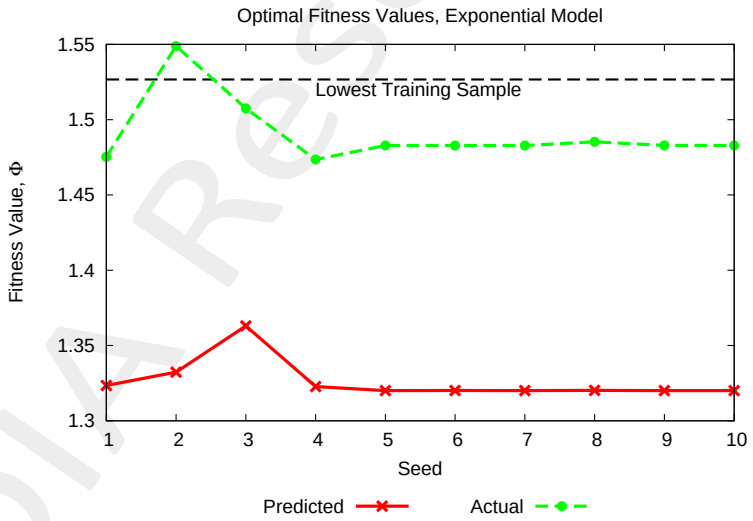

Figure 1: Predicted and actual fitness values vs seed. The lowest training sample is equal to $\Phi^{opt}_{train} = 1.53$.

1.0.3 Fitness vs iterations (seed 10)

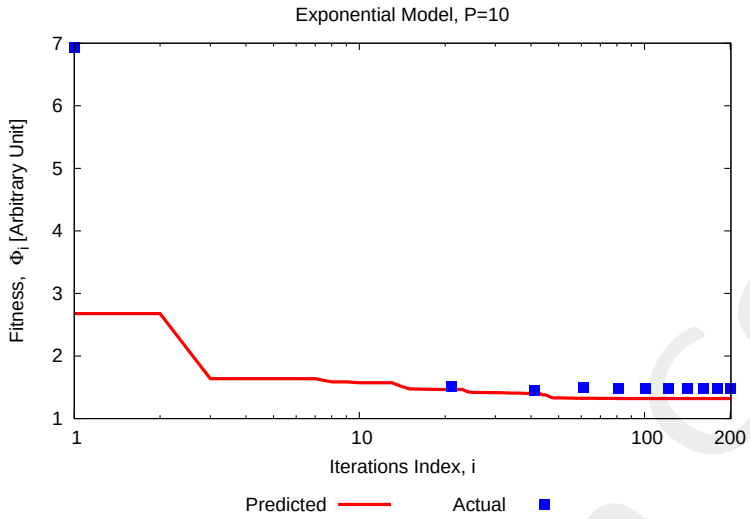

Figure 2: Total fitness evolution: comparison between the predicted and actual values.

1.0.4 Comparison between different prediction models

For comparative purposes, the synthesis has been performed by considering multiple regression and correlation models. More details, the following models

have been considered:

- Ordinary Kriging Regression Model with:
  - Exponential correlation model ($p = 1$);
  - Gaussian correlation model ($p = 2$);
  - Generalized Exponential correlation model (p is optimized);
- RBFN (Radial Basis Function Network);

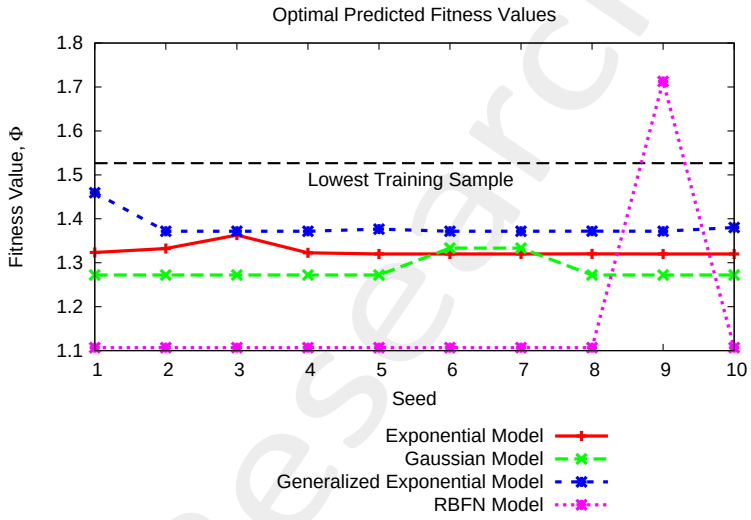

(a)

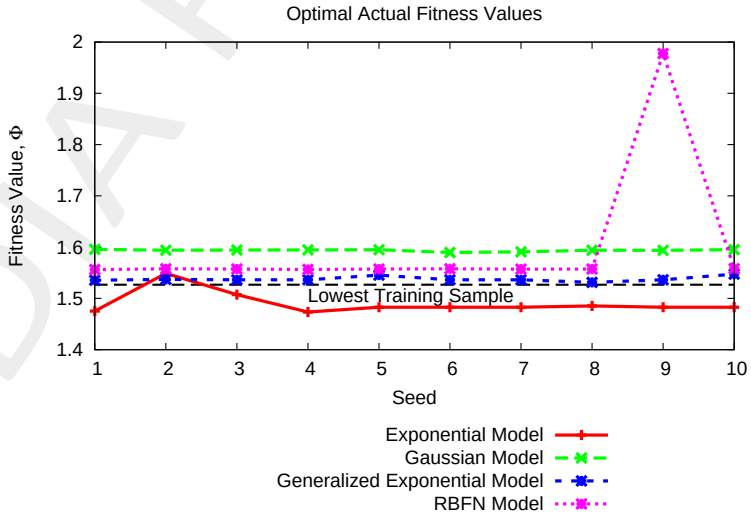

(b)

Figure 3: Comparison between the optimal fitness obtained by considering different correlation models for Kriging (i.e. Exponential, Gaussian, Generalized Exponential) and a RBFN predictor: (a) predicted fitness values and (b) actual fitness values.

1.0.5 (Semi)Exhaustive testing of the surrogate model

In this test the surrogate model (Exponential Correlation) has been tested in a (semi) exhaustive way in order to check if the PSO optimizer has been converged in the global minimum or in a local one. More in detail, the model has been tested in 10^5 locations: the objective is to compare the optimal predicted fitness of the best seed with the lowest functional value retrieved with this very fine sampling of the surrogate model.

- Best optimal predicted fitness value among the different seeds: $\widehat{\Phi}^{opt}_{best} = 1.32$
- Lowest fitness value obtained by testing the surrogate model in 10^5 random locations (generated via **LHS**): $\widehat{\Phi}^{opt}_{test} = 1.36$

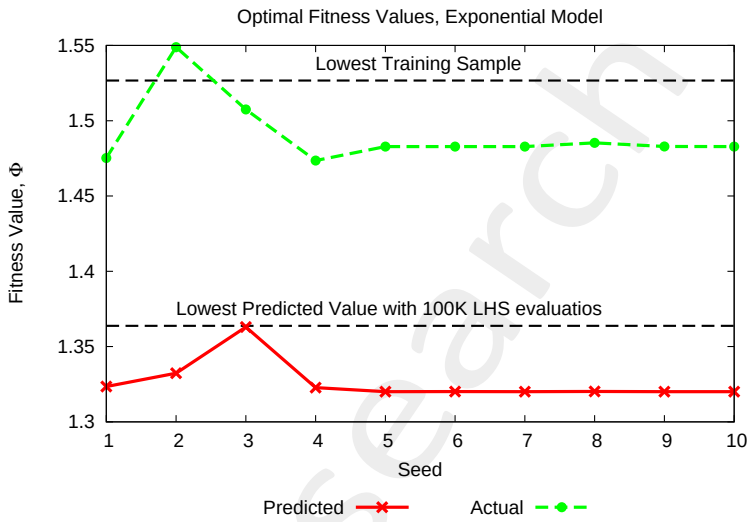

Figure 4: Predicted and actual fitness values vs seed. The lowest training sample is equal to $\Phi^{opt}_{train} = 1.53$, the lowest fitness value obtained by testing the surrogate model in 10^5 random locations is equal to $\widehat{\Phi}^{opt}_{test} = 1.36$ and the best optimal predicted fitness value among the different seeds is equal to $\widehat{\Phi}^{opt}_{best} = 1.32$.

1.0.6 Computational time for PSO optimization (Intel(R) Core(TM) i5 CPU 650 @ 3.20GHz, 4-GB-Ram)

- Time for training a Kriging surrogate model with $\tau = 250$ $K = 5$-dimensional training samples: $\Delta t^{train}|_{N=\tau=250} \simeq 1.25$ [sec];
- Time for testing $P = 10$ $K = 5$-dimensional trial solutions using a Kriging surrogate model (built on $\tau = 250$ training samples): $\Delta t^{test}|_{M=P=10} \simeq 1.50 \times 10^{-2}$ [sec];
- Real total duration of the optimization: $\Delta t^{tot} \simeq 26$ $[sec]$.

1.0.7 Analysis of the Optimized Solution (Seed 10)

The optimal value of the radome spline parameters are summarized in the following table.

Parameter	Description	Optimized Value [m]	Min [m]	Max [m]
t_1	Radome thickness at the quota $z = z_1$	7.58×10^{-3}	6.56×10^{-3}	9.84×10^{-3}
t_2	Radome thickness at the quota $z = z_2$	7.31×10^{-3}	6.56×10^{-3}	9.84×10^{-3}
t_3	Radome thickness at the quota $z = z_3$	6.60×10^{-3}	6.56×10^{-3}	9.84×10^{-3}
t_4	Radome thickness at the quota $z = z_4$	7.00×10^{-3}	6.56×10^{-3}	9.84×10^{-3}
t_5	Radome thickness at the quota $z = z_5$	6.86×10^{-3}	6.56×10^{-3}	9.84×10^{-3}

Table IV: List of all considered boundaries for the optimized radome descriptors.

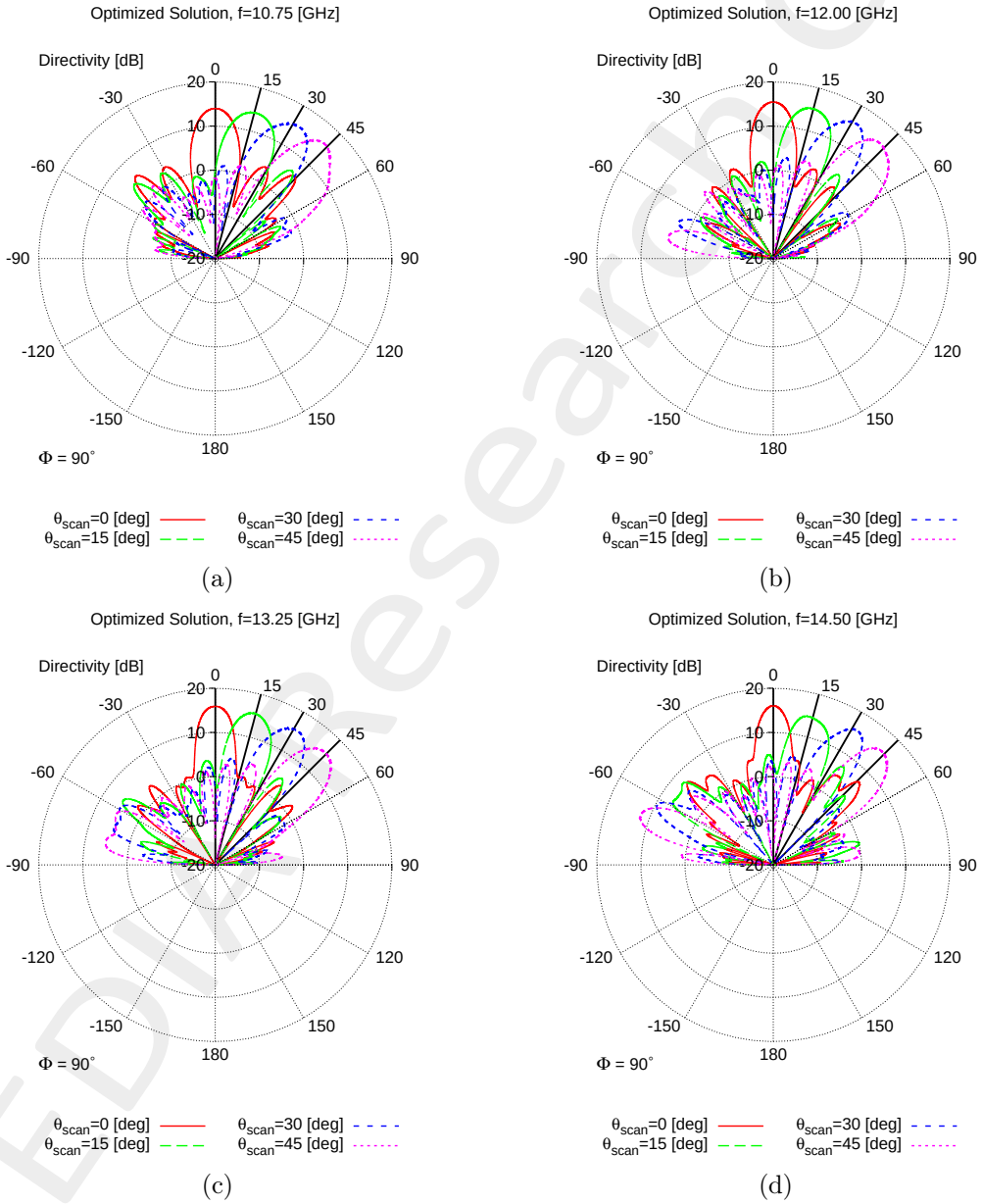

Figure 5: Radiated pattern for the optimized solution at (a) 10.75 $[GHz]$, (b) 12.00 $[GHz]$, (c) 13.25 $[GHz]$ and (d) 14.50 $[GHz]$.

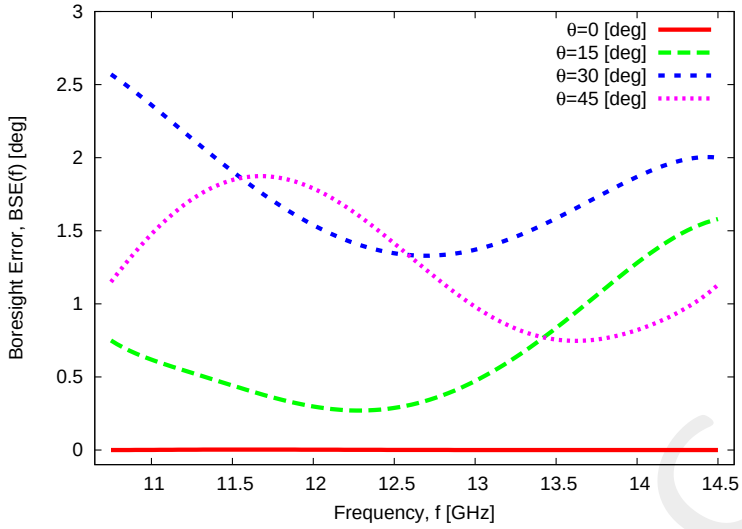

Figure 6: Pointing error vs frequency.

	$\theta_j = 0.0$ $[deg]$		$\theta_j = 15.0$ $[deg]$		$\theta_j = 30.0$ $[deg]$		$\theta_j = 45.0$ $[deg]$	
Frequency f_n $[GHz]$	$\widehat{\theta}_i$ $[deg]$	$\lvert\widehat{\theta}_i - \theta_j\rvert$ $[deg]$	$\widehat{\theta}_i$ $[deg]$	$\lvert\widehat{\theta}_i - \theta_j\rvert$ $[deg]$	$\widehat{\theta}_i$ $[deg]$	$\lvert\widehat{\theta}_i - \theta_j\rvert$ $[deg]$	$\widehat{\theta}_i$ $[deg]$	$\lvert\widehat{\theta}_i - \theta_j\rvert$ $[deg]$
10.75	0.00	0.00	1.57×10^1	7.50×10^{-1}	3.26×10^1	2.57	4.39×10^1	1.15
11.17	0.00	0.00	1.54×10^1	4.50×10^{-1}	3.23×10^1	2.26	4.33×10^1	1.75
11.58	0.00	0.00	1.56×10^1	5.90×10^{-1}	3.18×10^1	1.75	4.28×10^1	2.20
12.00	0.00	0.00	1.49×10^1	1.10×10^{-1}	3.14×10^1	1.43	4.29×10^1	2.10
12.42	0.00	0.00	1.50×10^1	1.00×10^{-2}	3.12×10^1	1.17	4.32×10^1	1.79
12.83	0.00	0.00	1.47×10^1	3.30×10^{-1}	3.10×10^1	1.03	4.42×10^1	8.20×10^{-1}
13.25	0.00	0.00	1.46×10^1	3.70×10^{-1}	3.14×10^1	1.41	4.47×10^1	3.30×10^{-1}
13.67	0.00	0.00	1.40×10^1	1.04	3.17×10^1	1.65	4.42×10^1	8.00×10^{-1}
14.08	0.00	0.00	1.35×10^1	1.47	3.21×10^1	2.06	4.43×10^1	7.10×10^{-1}
14.50	0.00	0.00	1.34×10^1	1.58	3.20×10^1	2.00	4.39×10^1	1.13

Table V: Pointing directions and pointing error of the optimized solution.

1.0.8 Comparison between the optimized solution and a standard ogive radome with constant thickness profile

In order to show the improvement introduced by the spline-based radome, the performances of the optimized radome have been compared with the performances of a standard ogive radome with constant thickness profile. The thickness profile are shown in Figure (7), while the functional value of the two solutions is provided in the following:

- optimized spline radome: $\Phi^{opt} = 1.48$
- constant thickness radome (the thickness of the radome is equal to $t_0 = 8.20 \times 10^{-3}$ $[m]$): $\Phi = 4.77$

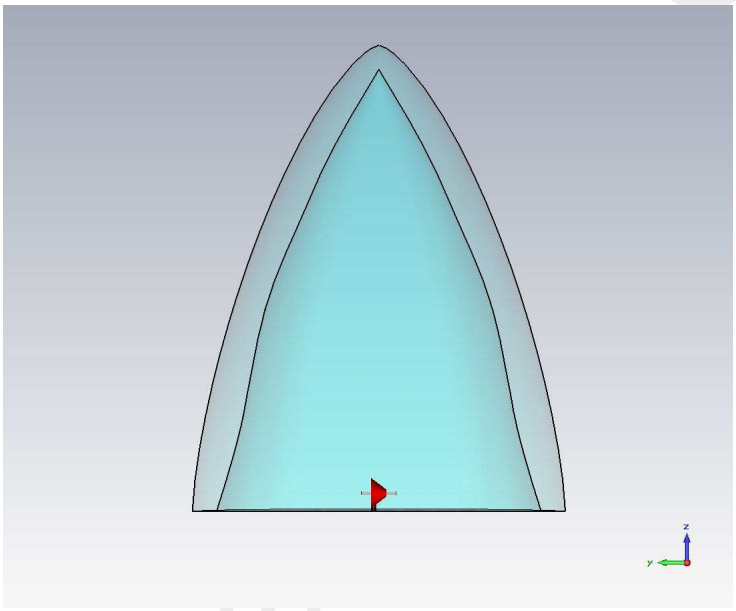

(a) - spline radome

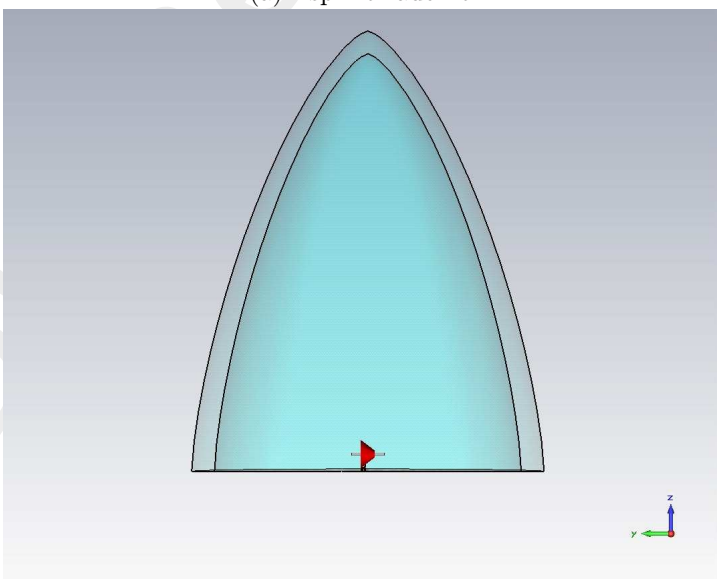

(b) - constant thickness radome

Figure 7: Plot of (a) the optimized radome profile and (b) a constant thickness radome.

Patterns for $\theta_j = 0.0$ $[deg]$

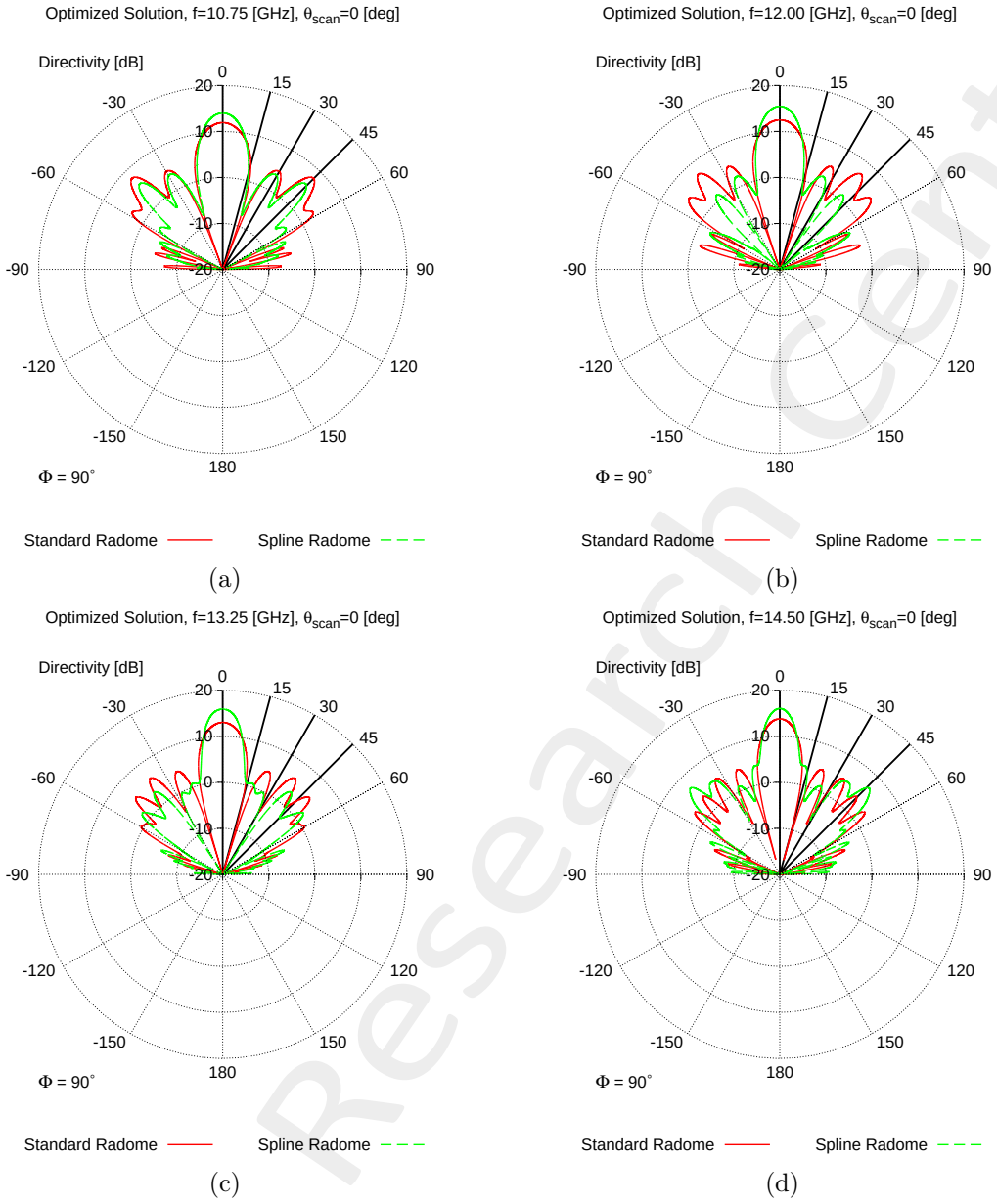

Figure 8: Comparison between the pattern radiated by the array with a standard ogive radome with constant thickness (red curve) and with the optimized ogive radome (green curve) at (a) 10.75 $[GHz]$, (b) 12.00 $[GHz]$, (c) 13.25 $[GHz]$ and (d) 14.50 $[GHz]$ (Scanning angle $\theta = \theta_1 = 0.0$ $[deg]$).

$\theta_j = 0.0\ [deg]$				
	Standard Radome		Spline Radome	
Frequency $f_n\ [GHz]$	$\widehat{\theta}_i\ [deg]$	$\left\|\widehat{\theta}_i - \theta_j\right\|\ [deg]$	$\widehat{\theta}_i\ [deg]$	$\left\|\widehat{\theta}_i - \theta_j\right\|\ [deg]$
10.75	0.00	0.00	0.00	0.00
11.17	0.00	0.00	0.00	0.00
11.58	0.00	0.00	0.00	0.00
12.00	0.00	0.00	0.00	0.00
12.42	0.00	0.00	0.00	0.00
12.83	0.00	0.00	0.00	0.00
13.25	0.00	0.00	0.00	0.00
13.67	0.00	0.00	0.00	0.00
14.08	0.00	0.00	0.00	0.00
14.50	0.00	0.00	0.00	0.00

Table VI: Pointing directions and pointing error of the optimized solution: comparison between a constant thickness radome and the optimized spline-based radome.

Patterns for $\theta_j = 15.0\ [deg]$

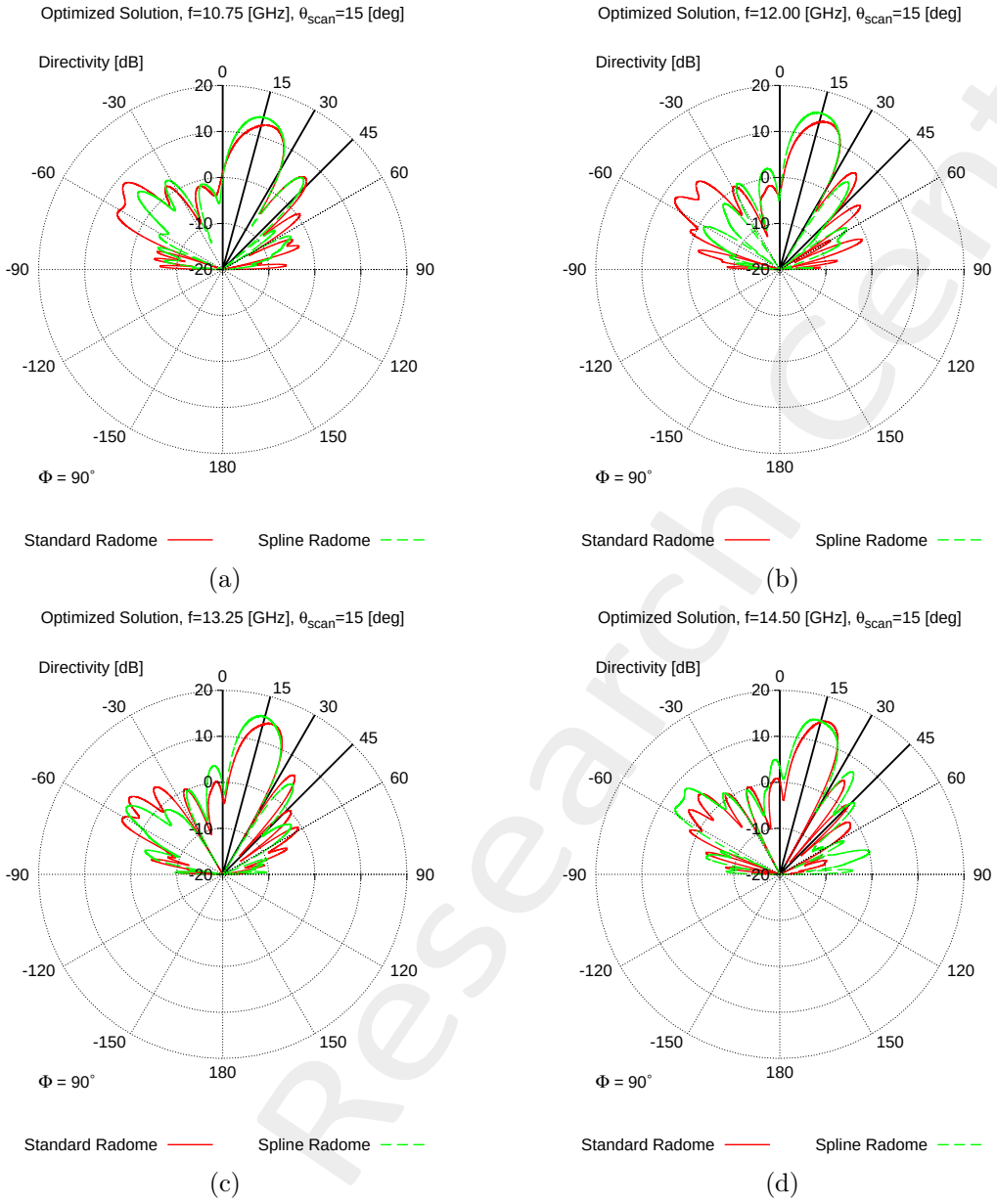

Figure 9: Comparison between the pattern radiated by the array with a standard ogive radome with constant thickness (red curve) and with the optimized ogive radome (green curve) at (a) 10.75 $[GHz]$, (b) 12.00 $[GHz]$, (c) 13.25 $[GHz]$ and (d) 14.50 $[GHz]$ (Scanning angle $\theta = \theta_2 = 15.0\ [deg]$).

$\theta_j = 15.0\ [deg]$				
	Standard Radome		Spline Radome	
Frequency $f_n\ [GHz]$	$\widehat{\theta}_i\ [deg]$	$\left\|\widehat{\theta}_i - \theta_j\right\|\ [deg]$	$\widehat{\theta}_i\ [deg]$	$\left\|\widehat{\theta}_i - \theta_j\right\|\ [deg]$
10.75	1.89×10^1	3.87	1.57×10^1	7.50×10^{-1}
11.17	1.85×10^1	3.51	1.54×10^1	4.50×10^{-1}
11.58	1.86×10^1	3.65	1.56×10^1	5.90×10^{-1}
12.00	1.83×10^1	3.31	1.49×10^1	1.10×10^{-1}
12.42	1.86×10^1	3.57	1.50×10^1	1.00×10^{-2}
12.83	1.85×10^1	3.55	1.47×10^1	3.30×10^{-1}
13.25	1.83×10^1	3.30	1.46×10^1	3.70×10^{-1}
13.67	1.77×10^1	2.71	1.40×10^1	1.04
14.08	1.74×10^1	2.41	1.35×10^1	1.47
14.50	1.75×10^1	2.52	1.34×10^1	1.58

Table VII: Pointing directions and pointing error of the optimized solution: comparison between a constant thickness radome and the optimized spline-based radome.

Patterns for $\theta_j = 30.0\ [deg]$

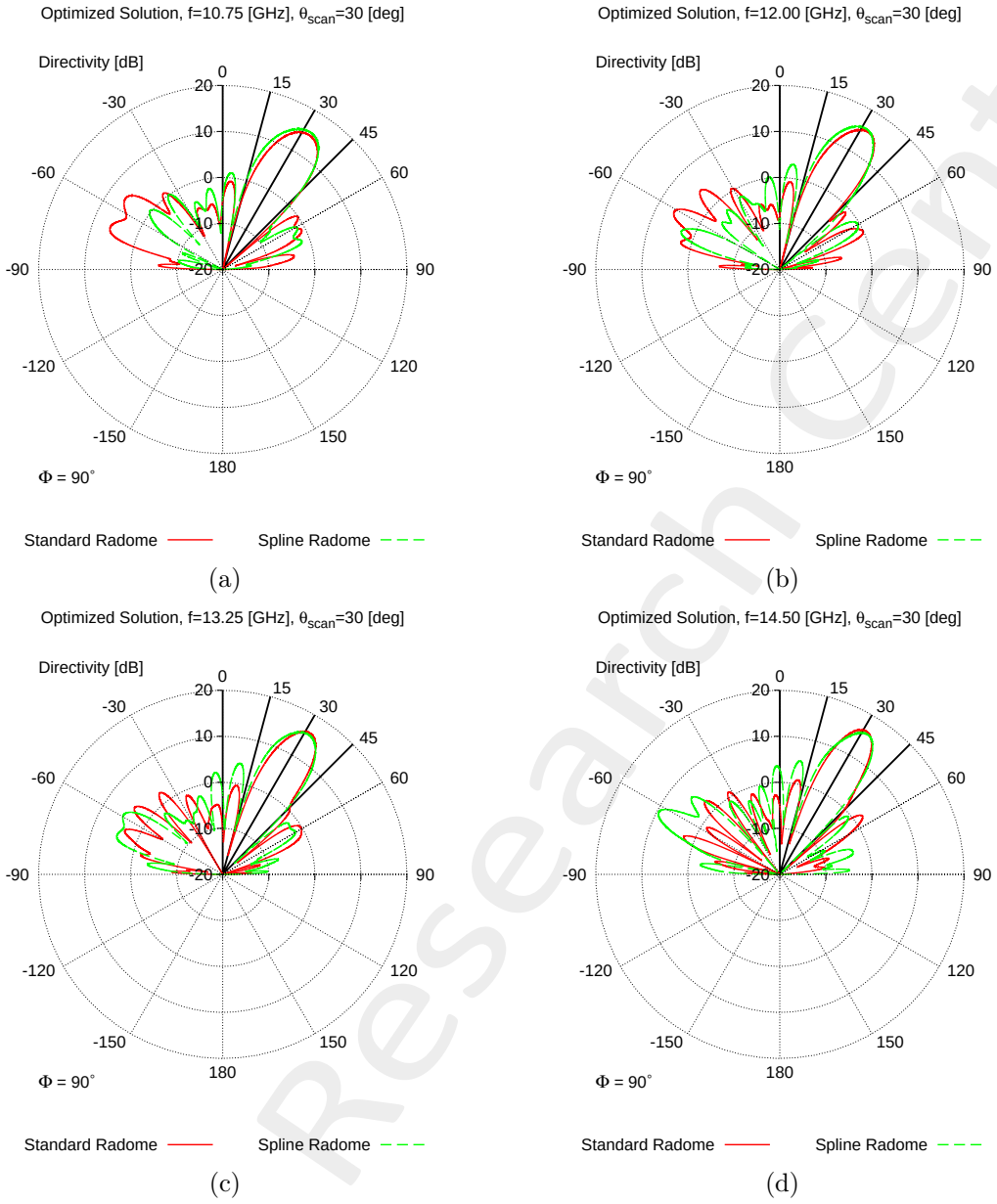

Figure 10: Comparison between the pattern radiated by the array with a standard ogive radome with constant thickness (red curve) and with the optimized ogive radome (green curve) at (a) 10.75 $[GHz]$, (b) 12.00 $[GHz]$, (c) 13.25 $[GHz]$ and (d) 14.50 $[GHz]$ (Scanning angle $\theta = \theta_3 = 30.0\ [deg]$).

$\theta_j = 30.0\ [deg]$				
	Standard Radome		Spline Radome	
Frequency $f_n\ [GHz]$	$\widehat{\theta}_i\ [deg]$	$\left\|\widehat{\theta}_i - \theta_j\right\|\ [deg]$	$\widehat{\theta}_i\ [deg]$	$\left\|\widehat{\theta}_i - \theta_j\right\|\ [deg]$
10.75	3.27×10^1	2.67	3.26×10^1	2.57
11.17	3.31×10^1	3.07	3.23×10^1	2.26
11.58	3.28×10^1	2.80	3.18×10^1	1.75
12.00	3.28×10^1	2.76	3.14×10^1	1.43
12.42	3.23×10^1	2.28	3.12×10^1	1.17
12.83	3.21×10^1	2.07	3.10×10^1	1.03
13.25	3.18×10^1	1.78	3.14×10^1	1.41
13.67	3.13×10^1	1.34	3.17×10^1	1.65
14.08	3.14×10^1	1.39	3.21×10^1	2.06
14.50	3.11×10^1	1.12	3.20×10^1	2.00

Table VIII: Pointing directions and pointing error of the optimized solution: comparison between a constant thickness radome and the optimized spline-based radome.

Patterns for $\theta_j = 45.0\ [deg]$

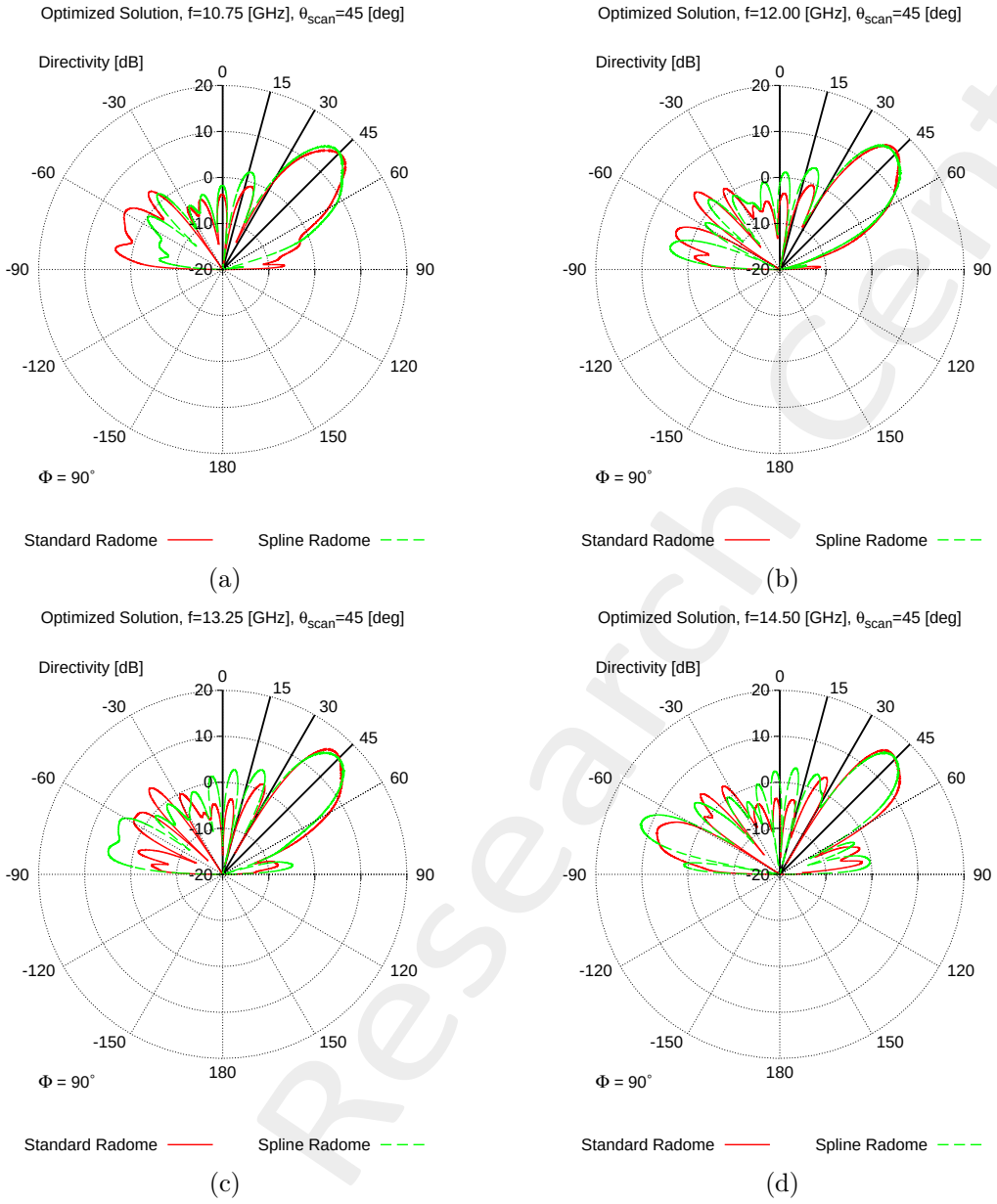

Figure 11: Comparison between the pattern radiated by the array with a standard ogive radome with constant thickness (red curve) and with the optimized ogive radome (green curve) at (a) 10.75 $[GHz]$, (b) 12.00 $[GHz]$, (c) 13.25 $[GHz]$ and (d) 14.50 $[GHz]$ (Scanning angle $\theta = \theta_4 = 45.0\ [deg]$).

$\theta_j = 45.0\ [deg]$				
	Standard Radome		Spline Radome	
Frequency $f_n\ [GHz]$	$\widehat{\theta_i}\ [deg]$	$\left\|\widehat{\theta_i} - \theta_j\right\|\ [deg]$	$\widehat{\theta_i}\ [deg]$	$\left\|\widehat{\theta_i} - \theta_j\right\|\ [deg]$
10.75	4.62×10^1	1.20	4.39×10^1	1.15
11.17	4.45×10^1	4.50×10^{-1}	4.33×10^1	1.75
11.58	4.41×10^1	9.10×10^{-1}	4.28×10^1	2.20
12.00	4.36×10^1	1.40	4.29×10^1	2.10
12.42	4.30×10^1	1.97	4.32×10^1	1.79
12.83	4.28×10^1	2.19	4.42×10^1	8.20×10^{-1}
13.25	4.27×10^1	2.26	4.47×10^1	3.30×10^{-1}
13.67	4.27×10^1	2.27	4.42×10^1	8.00×10^{-1}
14.08	4.28×10^1	2.17	4.43×10^1	7.10×10^{-1}
14.50	4.26×10^1	2.39	4.39×10^1	1.13

Table IX: Pointing directions and pointing error of the optimized solution: comparison between a constant thickness radome and the optimized spline-based radome.

Resume

This section reports the pointing error vs frequency and scanning angle for the standard constant thickness radome and the optimized spline-based radome.

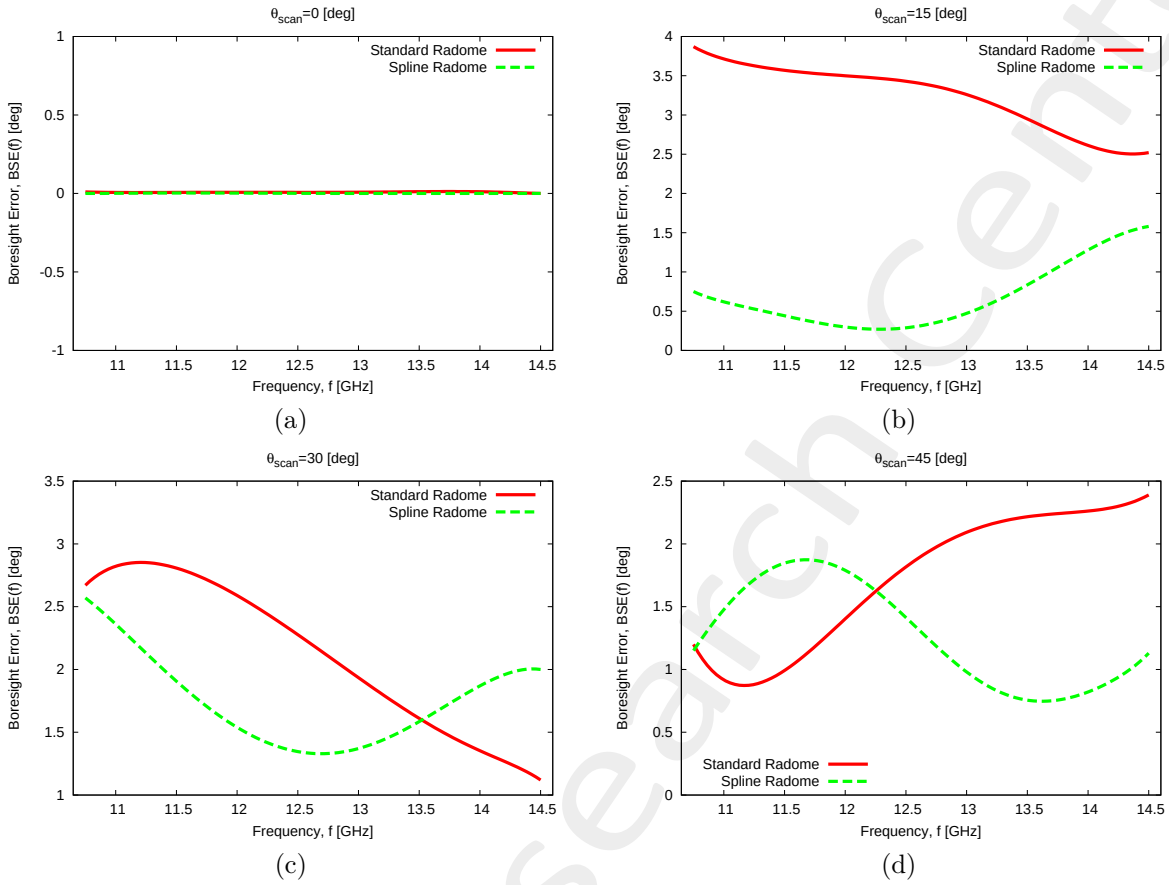

Figure 12: Pointing error vs frequency: comparison between a constant thickness radome and the optimized spline-based radome at (a) 10.75 $[GHz]$, (b) 12.00 $[GHz]$, (c) 13.25 $[GHz]$ and (d) 14.50 $[GHz]$.

2 Optimization with SADE

2.0.1 *SADE* parameters

- Number of variables: $K = 5$;
- Population dimension: $P = 50$;
- Scaling factor: $Q = 0.6$;
- Crossover probability: $P_c = 0.8$;
- Primary parent selection mode: $SADE/RAND/1$;
- Maximum number of iterations: $I = 200$;
- Fitness threshold: $\Phi^{th} = 10^{-20}$;
- Dimension of the training set: $\tau = 50^{(1)}$;
- Initialization strategy: ELEDIA (random P individuals + $(\tau - P)$ generated via LHS);
- Pre-screening strategy: LCB, $\omega = 2$;
- Update strategy: most promising individual overwrites itself;
- Random seed: $S = 1$;

Parameter	**Description**	**Optimized Value [m]**	Min [m]	Max [m]
t_1	Radome thickness at the quota $z = z_1$	8.12×10^{-3}	6.56×10^{-3}	9.84×10^{-3}
t_2	Radome thickness at the quota $z = z_2$	6.63×10^{-3}	6.56×10^{-3}	9.84×10^{-3}
t_3	Radome thickness at the quota $z = z_3$	6.57×10^{-3}	6.56×10^{-3}	9.84×10^{-3}
t_4	Radome thickness at the quota $z = z_4$	6.56×10^{-3}	6.56×10^{-3}	9.84×10^{-3}
t_5	Radome thickness at the quota $z = z_5$	7.32×10^{-3}	6.56×10^{-3}	9.84×10^{-3}

Table X: List of all considered boundaries for the optimized radome descriptors: **narrow bounds**.

Parameter	**Description**	**Optimized Value [m]**	Min [m]	Max [m]
t_1	Radome thickness at the quota $z = z_1$	8.34×10^{-3}	3.28×10^{-3}	13.12×10^{-3}
t_2	Radome thickness at the quota $z = z_2$	5.07×10^{-3}	3.28×10^{-3}	13.12×10^{-3}
t_3	Radome thickness at the quota $z = z_3$	4.83×10^{-3}	3.28×10^{-3}	13.12×10^{-3}
t_4	Radome thickness at the quota $z = z_4$	4.65×10^{-3}	3.28×10^{-3}	13.12×10^{-3}
t_5	Radome thickness at the quota $z = z_5$	1.04×10^{-2}	3.28×10^{-3}	13.12×10^{-3}

Table XI: List of all considered boundaries for the optimized radome descriptors: **wide bounds (WB).**

[(1)] Note that the dimension of the training set is much lower than the training set used for the PSO. This choice is motivated by the fact that during the optimization the $SADE$ computes one new training sample at each iteration. The final number of performed simulations is then equal to $\tau + I = 50 + 200 = 250$.

2.0.2 Fitness

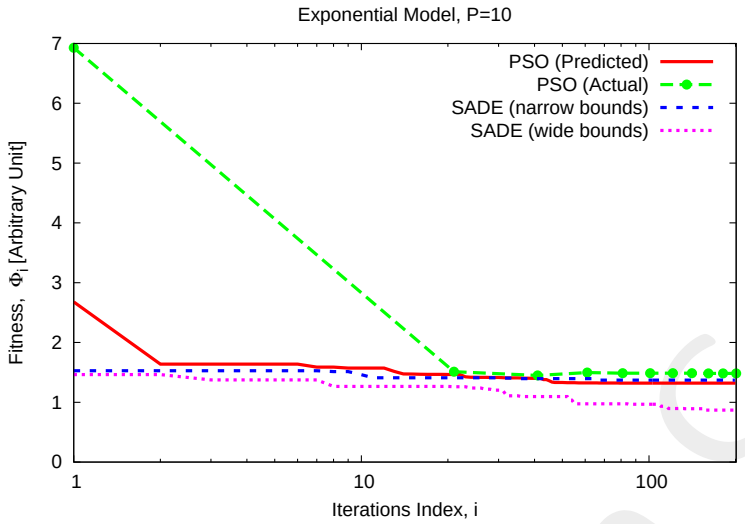

Figure 13: Total fitness evolution: comparison between PSO (predicted and actual values). $\Phi^{opt}_{PSO} = 1.48$, $\Phi^{opt}_{SADE,NB} = 1.37$, $\Phi^{opt}_{SADE,WB} = 0.87$.

2.0.3 Analysis of the Optimized Solution

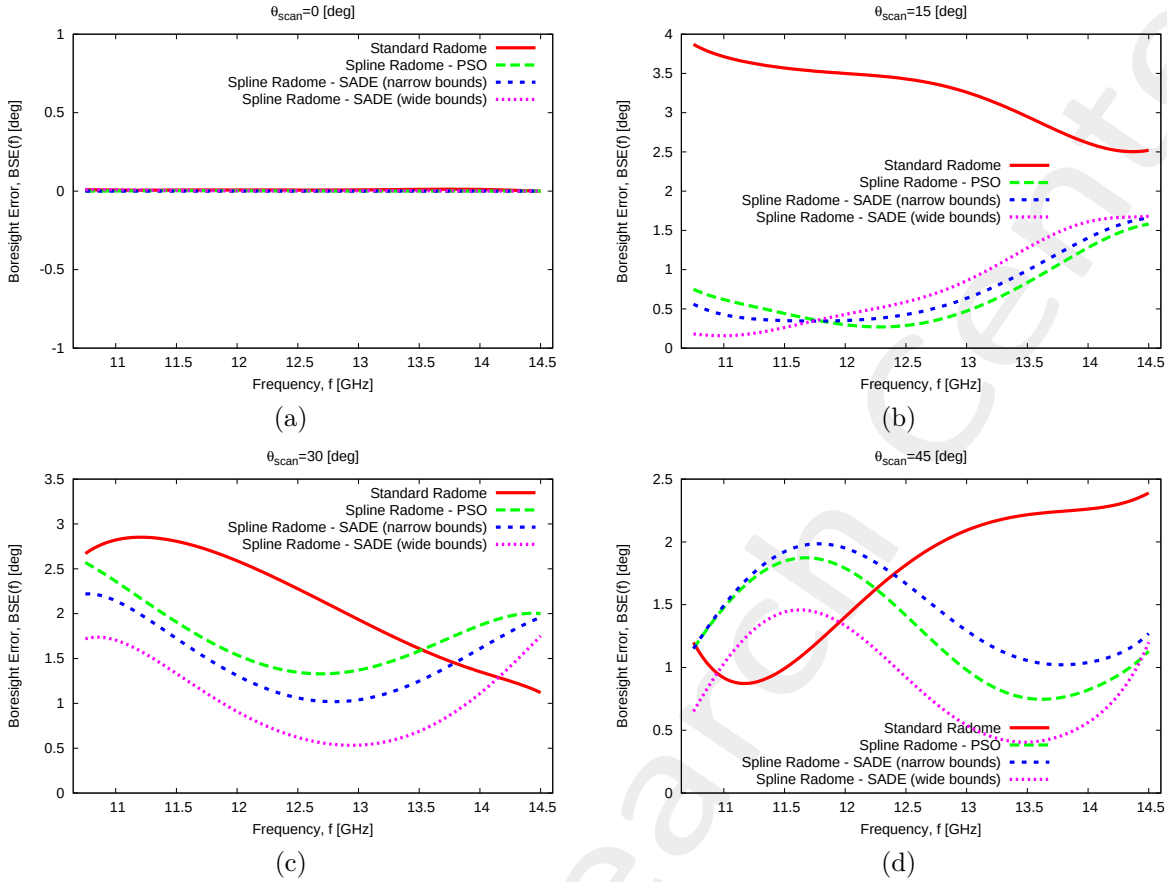

Table XII: Pointing error vs frequency: comparison between a constant thickness radome and the optimized spline-based radome at (a) 10.75 $[GHz]$, (b) 12.00 $[GHz]$, (c) 13.25 $[GHz]$ and (d) 14.50 $[GHz]$.

Patterns for $\theta_j = 0.0$ $[deg]$

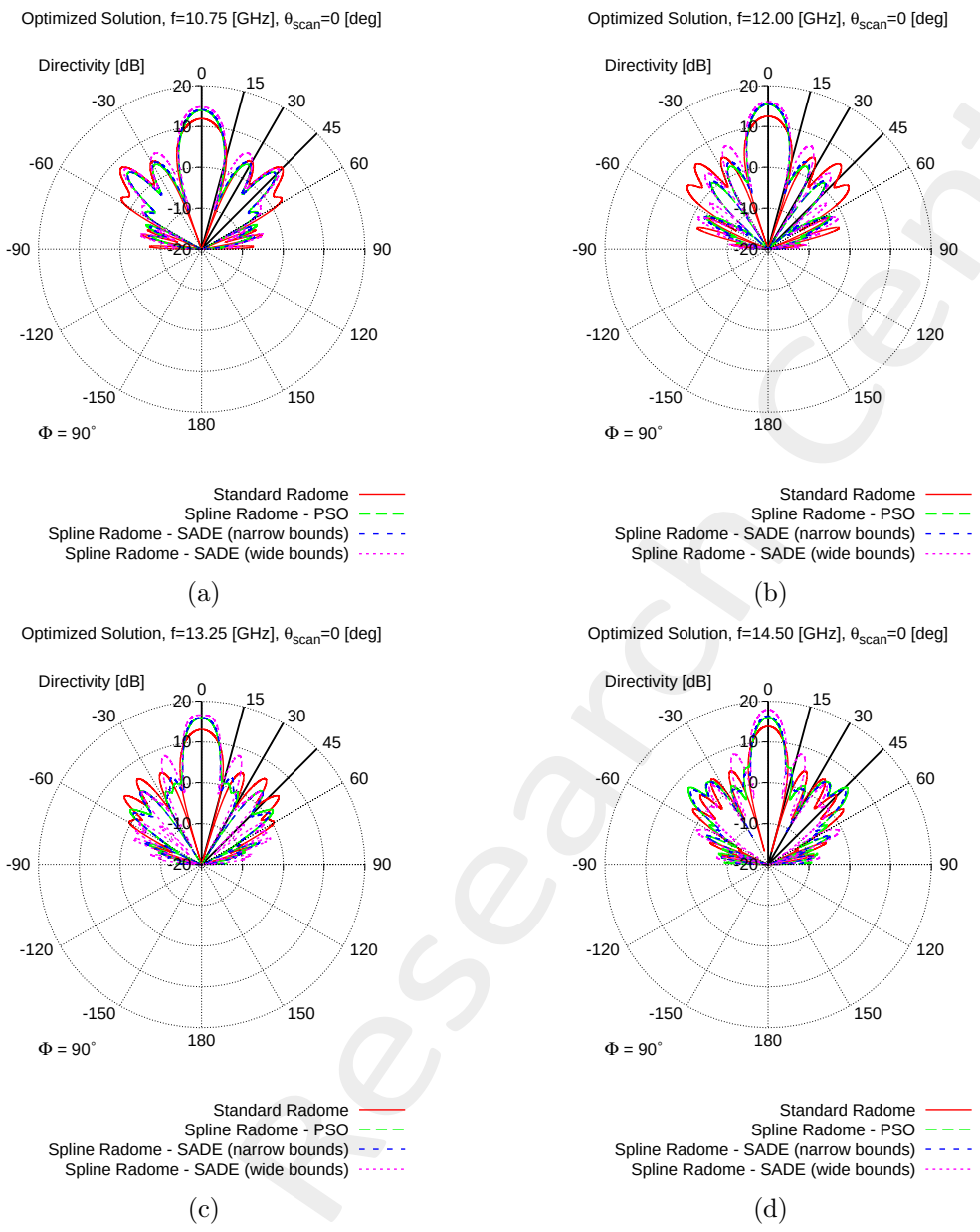

Figure 14: Comparison between the pattern radiated by the array with a standard ogive radome with constant thickness (red curve) and with the optimized ogive radome (green curve) at (a) 10.75 $[GHz]$, (b) 12.00 $[GHz]$, (c) 13.25 $[GHz]$ and (d) 14.50 $[GHz]$ (Scanning angle $\theta = \theta_1 = 0.0$ $[deg]$).

$\theta_j = 0.0$ $[deg]$								
	Standard Radome		Spline - PSO		Spline - SADE (NB)		Spline - SADE (WB)	
Frequency f_n $[GHz]$	$\widehat{\theta}_i$ $[deg]$	$\lvert\widehat{\theta}_i - \theta_j\rvert$ $[deg]$	$\widehat{\theta}_i$ $[deg]$	$\lvert\widehat{\theta}_i - \theta_j\rvert$ $[deg]$	$\widehat{\theta}_i$ $[deg]$	$\lvert\widehat{\theta}_i - \theta_j\rvert$ $[deg]$	$\widehat{\theta}_i$ $[deg]$	$\lvert\widehat{\theta}_i - \theta_j\rvert$ $[deg]$
10.75	0.00	0.00	0.00	0.00	0.00	0.00	0.00	0.00
11.17	0.00	0.00	0.00	0.00	0.00	0.00	0.00	0.00
11.58	0.00	0.00	0.00	0.00	0.00	0.00	0.00	0.00
12.00	0.00	0.00	0.00	0.00	0.00	0.00	0.00	0.00
12.42	0.00	0.00	0.00	0.00	0.00	0.00	0.00	0.00
12.83	0.00	0.00	0.00	0.00	0.00	0.00	0.00	0.00
13.25	0.00	0.00	0.00	0.00	0.00	0.00	0.00	0.00
13.67	0.00	0.00	0.00	0.00	0.00	0.00	0.00	0.00
14.08	0.00	0.00	0.00	0.00	0.00	0.00	0.00	0.00
14.50	0.00	0.00	0.00	0.00	0.00	0.00	0.00	0.00

Table XIII: Pointing directions and pointing error of the optimized solution: comparison between a constant thickness radome and the optimized spline-based radome.

Patterns for $\theta_j = 15.0\ [deg]$

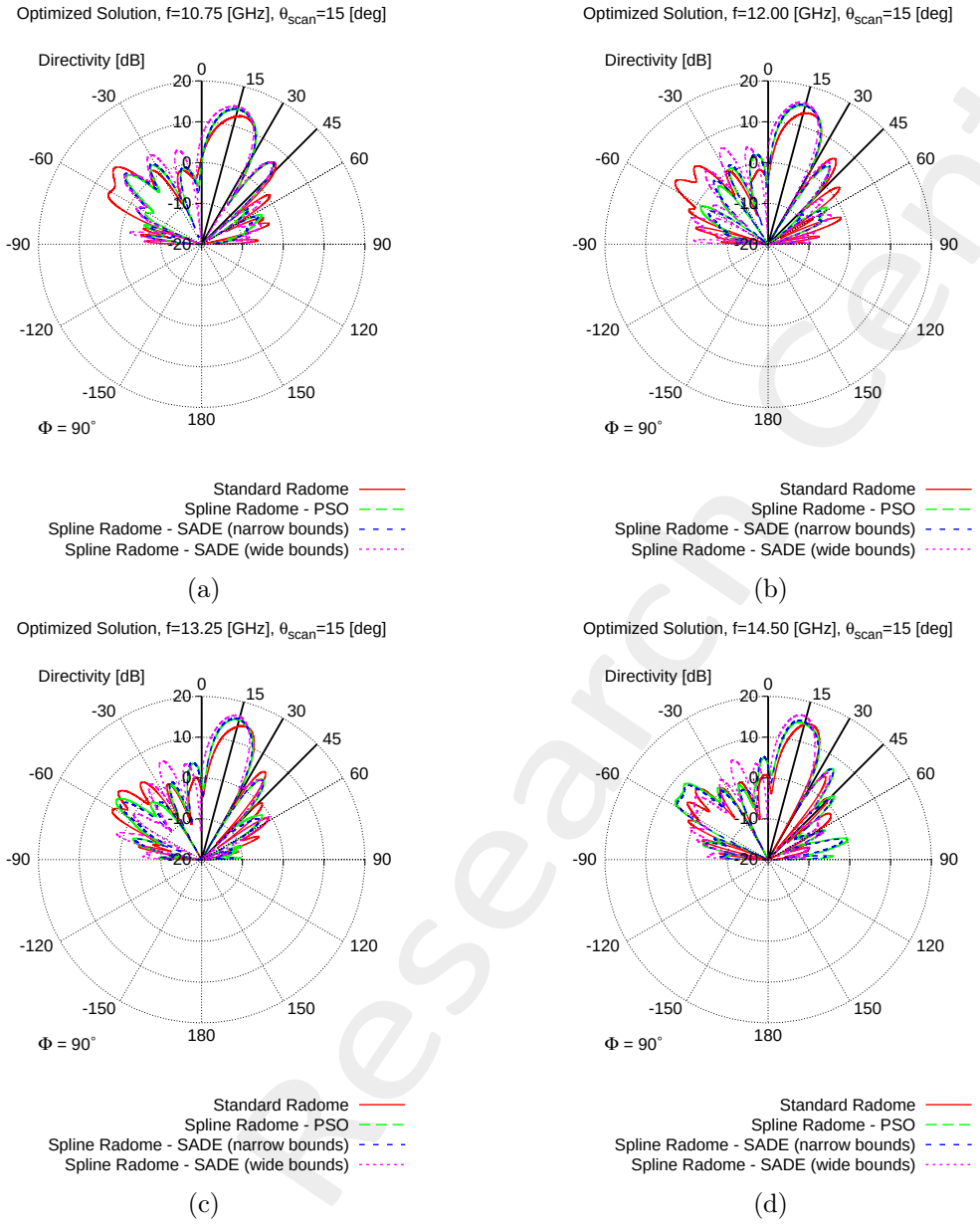

Figure 15: Comparison between the pattern radiated by the array with a standard ogive radome with constant thickness (red curve) and with the optimized ogive radome (green curve) at (a) 10.75 $[GHz]$, (b) 12.00 $[GHz]$, (c) 13.25 $[GHz]$ and (d) 14.50 $[GHz]$ (Scanning angle $\theta = \theta_2 = 15.0\ [deg]$).

$\theta_j = 15.0\ [deg]$								
	Standard Radome		Spline - PSO		Spline - SADE (N.B.)		Spline - SADE (W.B.)	
Frequency f_n $[GHz]$	$\widehat{\theta}_i$ $[deg]$	$\lvert\widehat{\theta}_i - \theta_j\rvert$ $[deg]$	$\widehat{\theta}_i$ $[deg]$	$\lvert\widehat{\theta}_i - \theta_j\rvert$ $[deg]$	$\widehat{\theta}_i$ $[deg]$	$\lvert\widehat{\theta}_i - \theta_j\rvert$ $[deg]$	$\widehat{\theta}_i$ $[deg]$	$\lvert\widehat{\theta}_i - \theta_j\rvert$ $[deg]$
10.75	1.89×10^1	3.87	1.57×10^1	7.50×10^{-1}	1.56×10^1	5.60×10^{-1}	1.52×10^1	1.80×10^{-1}
11.17	1.85×10^1	3.51	1.54×10^1	4.50×10^{-1}	1.52×10^1	2.30×10^{-1}	1.51×10^1	1.20×10^{-1}
11.58	1.86×10^1	3.65	1.56×10^1	5.90×10^{-1}	1.54×10^1	4.00×10^{-1}	1.49×10^1	5.00×10^{-2}
12.00	1.83×10^1	3.31	1.49×10^1	1.10×10^{-1}	1.47×10^1	3.50×10^{-1}	1.41×10^1	8.50×10^{-1}
12.42	1.86×10^1	3.57	1.50×10^1	1.00×10^{-2}	1.48×10^1	2.10×10^{-1}	1.46×10^1	4.40×10^{-1}
12.83	1.85×10^1	3.55	1.47×10^1	3.30×10^{-1}	1.45×10^1	4.80×10^{-1}	1.47×10^1	3.00×10^{-1}
13.25	1.83×10^1	3.30	1.46×10^1	3.70×10^{-1}	1.45×10^1	0.53	1.41×10^1	9.00×10^{-1}
13.67	1.77×10^1	2.71	1.40×10^1	1.04	1.38×10^1	1.24	1.31×10^1	1.89
14.08	1.74×10^1	2.41	1.35×10^1	1.47	1.34×10^1	1.57	1.34×10^1	1.62
14.50	1.75×10^1	2.52	1.34×10^1	1.58	1.33×10^1	1.66	1.33×10^1	1.68

Table XIV: Pointing directions and pointing error of the optimized solution: comparison between a constant thickness radome and the optimized spline-based radome.

Patterns for $\theta_j = 30.0\ [deg]$

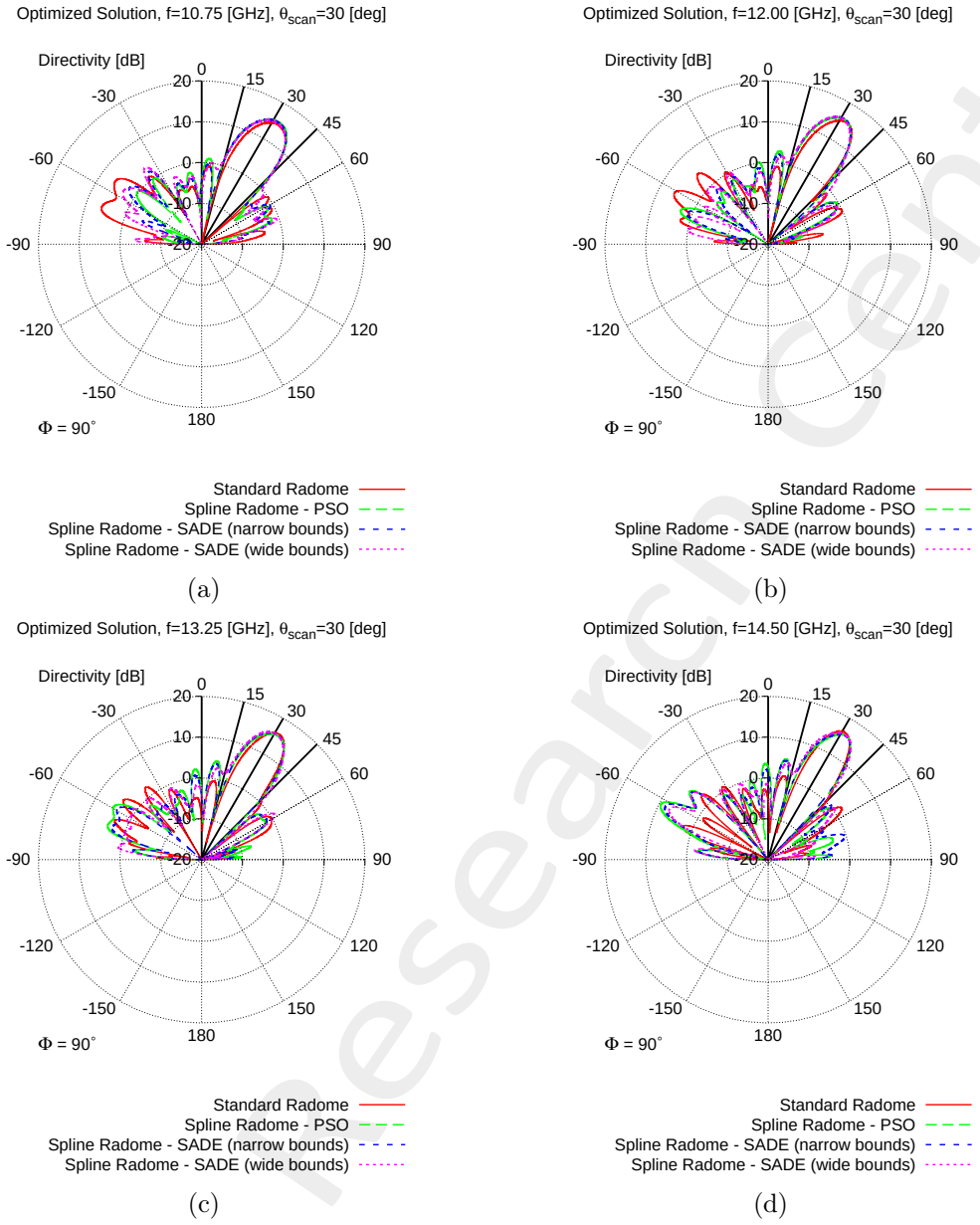

Figure 16: Comparison between the pattern radiated by the array with a standard ogive radome with constant thickness (red curve) and with the optimized ogive radome (green curve) at (a) 10.75 $[GHz]$, (b) 12.00 $[GHz]$, (c) 13.25 $[GHz]$ and (d) 14.50 $[GHz]$ (Scanning angle $\theta = \theta_3 = 30.0\ [deg]$).

$\theta_j = 30.0\ [deg]$								
	Standard Radome		Spline - PSO		Spline - SADE (N.B.)		Spline - SADE (W.B.)	
Frequency f_n $[GHz]$	$\widehat{\theta}_i$ $[deg]$	$\lvert\widehat{\theta}_i - \theta_j\rvert$ $[deg]$	$\widehat{\theta}_i$ $[deg]$	$\lvert\widehat{\theta}_i - \theta_j\rvert$ $[deg]$	$\widehat{\theta}_i$ $[deg]$	$\lvert\widehat{\theta}_i - \theta_j\rvert$ $[deg]$	$\widehat{\theta}_i$ $[deg]$	$\lvert\widehat{\theta}_i - \theta_j\rvert$ $[deg]$
10.75	3.27×10^1	2.67	3.26×10^1	2.57	3.22×10^1	2.22	3.17×10^1	1.72
11.17	3.31×10^1	3.07	3.23×10^1	2.26	3.23×10^1	2.26	3.19×10^1	1.88
11.58	3.28×10^1	2.80	3.18×10^1	1.75	3.15×10^1	1.50	3.12×10^1	1.19
12.00	3.28×10^1	2.76	3.14×10^1	1.43	3.12×10^1	1.23	3.08×10^1	7.60×10^{-1}
12.42	3.23×10^1	2.28	3.12×10^1	1.17	3.09×10^1	8.80×10^{-1}	3.05×10^1	5.30×10^{-1}
12.83	3.21×10^1	2.07	3.10×10^1	1.03	3.07×10^1	7.50×10^{-1}	3.03×10^1	2.90×10^{-1}
13.25	3.18×10^1	1.78	3.14×10^1	1.41	3.09×10^1	9.30×10^{-1}	3.04×10^1	4.10×10^{-1}
13.67	3.13×10^1	1.34	3.17×10^1	1.65	3.13×10^1	1.33×10^{-1}	3.06×10^1	5.70×10^{-1}
14.08	3.14×10^1	1.39	3.21×10^1	2.06	3.17×10^1	1.73×10^{-1}	3.12×10^1	1.18
14.50	3.11×10^1	1.12	3.20×10^1	2.00	3.20×10^1	1.96×10^{-1}	3.18×10^1	1.75

Table XV: Pointing directions and pointing error of the optimized solution: comparison between a constant thickness radome and the optimized spline-based radome.

Patterns for $\theta_j = 45.0\ [deg]$

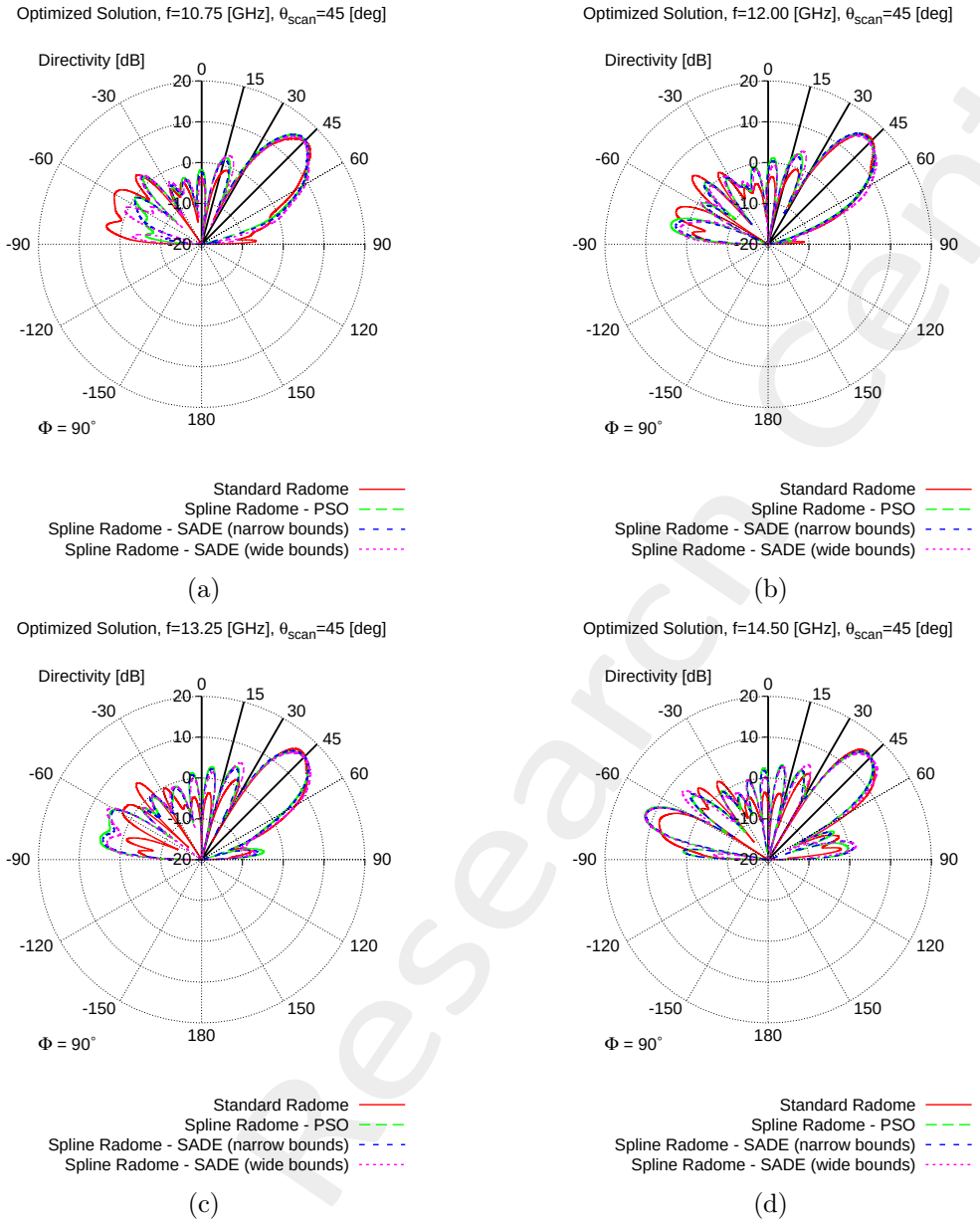

Figure 17: Comparison between the pattern radiated by the array with a standard ogive radome with constant thickness (red curve) and with the optimized ogive radome (green curve) at (a) 10.75 $[GHz]$, (b) 12.00 $[GHz]$, (c) 13.25 $[GHz]$ and (d) 14.50 $[GHz]$ (Scanning angle $\theta = \theta_3 = 45.0\ [deg]$).

$\theta_j = 45.0\ [deg]$								
	Standard Radome		Spline - PSO		Spline - SADE (N.B.)		Spline - SADE (W.B.)	
Frequency f_n $[GHz]$	$\widehat{\theta}_i$ $[deg]$	$\lvert\widehat{\theta}_i - \theta_j\rvert$ $[deg]$	$\widehat{\theta}_i$ $[deg]$	$\lvert\widehat{\theta}_i - \theta_j\rvert$ $[deg]$	$\widehat{\theta}_i$ $[deg]$	$\lvert\widehat{\theta}_i - \theta_j\rvert$ $[deg]$	$\widehat{\theta}_i$ $[deg]$	$\lvert\widehat{\theta}_i - \theta_j\rvert$ $[deg]$
10.75	4.62×10^1	1.20	4.39×10^1	1.15	4.39×10^1	1.15	4.44×10^1	6.50×10^{-1}
11.17	4.45×10^1	4.50×10^{-1}	4.33×10^1	1.75	4.32×10^1	1.77	4.37×10^1	1.34
11.58	4.41×10^1	9.10×10^{-1}	4.28×10^1	2.20	4.27×10^1	2.27	4.31×10^1	1.90
12.00	4.36×10^1	1.40	4.29×10^1	2.10	4.28×10^1	2.22	4.33×10^1	1.72
12.42	4.30×10^1	1.97	4.32×10^1	1.79	4.30×10^1	2.04	4.40×10^1	1.03
12.83	4.28×10^1	2.19	4.42×10^1	8.20×10^{-1}	4.38×10^1	1.21	4.47×10^1	2.60×10^{-1}
13.25	4.27×10^1	2.26	4.47×10^1	3.30×10^{-1}	4.43×10^1	7.20×10^{-1}	4.51×10^1	6.00×10^{-2}
13.67	4.27×10^1	2.27	4.42×10^1	8.00×10^{-1}	4.39×10^1	1.13	4.45×10^1	5.50×10^{-1}
14.08	4.28×10^1	2.17	4.43×10^1	7.10×10^{-1}	4.41×10^1	8.70×10^{-1}	4.48×10^1	2.30×10^{-1}
14.50	4.26×10^1	2.39	4.39×10^1	1.13	4.37×10^1	1.27	4.62×10^1	1.20

Table XVI: Pointing directions and pointing error of the optimized solution: comparison between a constant thickness radome and the optimized spline-based radome.

More information on the topics of this document can be found in the following list of references.

References

[1] A. Massa, D. Marcantonio, X. Chen, M. Li, and M. Salucci, "DNNs as applied to electromagnetics, antennas, and propagation - A review," *IEEE Antennas and Wirel. Propag. Lett.,* vol. 18, no. 11, pp. 2225-2229, Nov. 2019.

[2] A. Massa, G. Oliveri, M. Salucci, N. Anselmi, and P. Rocca, "Learning-by-examples techniques as applied to electromagnetics," *Journal of Electromagnetic Waves and Applications, Invited Review Article*, pp. 1-16, 2017.

[3] G. Oliveri, M. Salucci, and A. Massa, "Towards reflectarray digital twins - An EM-driven machine learning perspective," *IEEE Trans. Antennas Propag. - Special Issue on 'Machine Learning in Antenna Design, Modeling, and Measurements*', vol. 70, no. 7, pp. 5078-5093, July 2022.

[4] M. Salucci, L. Tenuti, G. Oliveri, and A. Massa, "Efficient prediction of the EM response of reflectarray antenna elements by an advanced statistical learning method," *IEEE Trans. Antennas Propag.*, vol. 66, no. 8, pp. 3995-4007, Aug. 2018.

[5] M. Salucci, G. Oliveri, M. A. Hannan, and A. Massa, "System-by-design paradigm-based synthesis of complex systems: The case of spline-contoured 3D radomes," *IEEE Antennas and Propagation Magazine - Special Issue on 'Artificial Intelligence in Electromagnetics*,', vol. 64, no. 1, pp. 72-83, Feb. 2022.

[6] G. Oliveri, P. Rocca, M. Salucci, and A. Massa, "Holographic smart EM skins for advanced beam power shaping in next generation wireless environments," *IEEE J. Multiscale Multiphysics Comput. Tech.*, vol. 6, pp. 171-182, Oct. 2021.

[7] G. Oliveri, A. Gelmini, A. Polo, N. Anselmi, and A. Massa, "System-by-design multi-scale synthesis of task-oriented reflectarrays," *IEEE Trans. Antennas Propag.*, vol. 68, no. 4, pp. 2867-2882, Apr. 2020.

[8] M. Salucci, L. Tenuti, G. Gottardi, A. Hannan, and A. Massa, "System-by-design method for efficient linear array miniaturisation through low-complexity isotropic lenses" *Electronic Letters*, vol. 55, no. 8, pp. 433-434, May 2019.

[9] M. Salucci, N. Anselmi, S. Goudos, and A. Massa, "Fast design of multiband fractal antennas through a system-by-design approach for NB-IoT applications," *EURASIP J. Wirel. Commun. Netw.*, vol. 2019, no. 1, pp. 68-83, Mar. 2019.

[10] M. Salucci, G. Oliveri, N. Anselmi, and A. Massa, "Material-by-design synthesis of conformal miniaturized linear phased arrays," *IEEE Access*, vol. 6, pp. 26367-26382, 2018.

[11] M. Salucci, G. Oliveri, N. Anselmi, G. Gottardi, and A. Massa, "Performance enhancement of linear active electronically-scanned arrays by means of MbD-synthesized metalenses," *Journal of Electromagnetic Waves and Applications*, vol. 32, no. 8, pp. 927-955, 2018.

[12] G. Oliveri, M. Salucci, N. Anselmi and A. Massa, "Multiscale System-by-Design synthesis of printed WAIMs for waveguide array enhancement," *IEEE J. Multiscale Multiphysics Computat. Techn.*, vol. 2, pp. 84-96, 2017.

[13] A. Massa and G. Oliveri, "Metamaterial-by-Design: Theory, methods, and applications to communications and sensing - Editorial," *EPJ Applied Metamaterials*, vol. 3, no. E1, pp. 1-3, 2016.

[14] G. Oliveri, F. Viani, N. Anselmi, and A. Massa, "Synthesis of multi-layer WAIM coatings for planar phased arrays within the system-by-design framework," *IEEE Trans. Antennas Propag.*, vol. 63, no. 6, pp. 2482-2496, June 2015.

[15] G. Oliveri, L. Tenuti, E. Bekele, M. Carlin, and A. Massa, "An SbD-QCTO approach to the synthesis of isotropic metamaterial lenses" *IEEE Antennas Wireless Propag. Lett.*, vol. 13, pp. 1783-1786, 2014.

[16] A. Massa, G. Oliveri, P. Rocca, and F. Viani, "System-by-Design: a new paradigm for handling design complexity," *8th European Conference on Antennas Propag. (EuCAP 2014), The Hague, The Netherlands*, pp. 1180-1183, Apr. 6-11, 2014.

[17] P. Rocca, M. Benedetti, M. Donelli, D. Franceschini, and A. Massa, "Evolutionary optimization as applied to inverse problems," *Inverse Problems - 25 th Year Special Issue of Inverse Problems, Invited Topical Review*, vol. 25, pp. 1-41, Dec. 2009.

[18] P. Rocca, G. Oliveri, and A. Massa, "Differential Evolution as applied to electromagnetics," *IEEE Antennas Propag. Mag.*, vol. 53, no. 1, pp. 38-49, Feb. 2011.

[19] P. Rocca, N. Anselmi, A. Polo, and A. Massa, "Pareto-optimal domino-tiling of orthogonal polygon phased arrays," *IEEE Trans. Antennas Propag.*, vol. 70, no. 5, pp. 3329-3342, May 2022.

[20] P. Rocca, N. Anselmi, A. Polo, and A. Massa, "An irregular two-sizes square tiling method for the design of isophoric phased arrays," *IEEE Trans. Antennas Propag.*, vol. 68, no. 6, pp. 4437-4449, Jun. 2020.

[21] P. Rocca, N. Anselmi, A. Polo, and A. Massa, "Modular design of hexagonal phased arrays through diamond tiles," *IEEE Trans. Antennas Propag.*, vol.68, no. 5, pp. 3598-3612, May 2020.

[22] N. Anselmi, L. Poli, P. Rocca, and A. Massa, "Design of simplified array layouts for preliminary experimental testing and validation of large AESAs," *IEEE Trans. Antennas Propag.*, vol. 66, no. 12, pp. 6906-6920, Dec. 2018.

[23] N. Anselmi, P. Rocca, M. Salucci, and A. Massa, "Contiguous phase-clustering in multibeam-on-receive scanning arrays," *IEEE Trans. Antennas Propag.*, vol. 66, no. 11, pp. 5879-5891, Nov. 2018.

[24] G. Oliveri, G. Gottardi, F. Robol, A. Polo, L. Poli, M. Salucci, M. Chuan, C. Massagrande, P. Vinetti, M. Mattivi, R. Lombardi, and A. Massa, "Co-design of unconventional array architectures and antenna elements for 5G base station," *IEEE Trans. Antennas Propag.*, vol. 65, no. 12, pp. 6752-6767, Dec. 2017.

[25] N. Anselmi, P. Rocca, M. Salucci, and A. Massa, "Irregular phased array tiling by means of analytic schemata-driven optimization," *IEEE Trans. Antennas Propag.*, vol. 65, no. 9, pp. 4495-4510, Sept. 2017.

[26] N. Anselmi, P. Rocca, M. Salucci, and A. Massa, "Optimization of excitation tolerances for robust beamforming in linear arrays" *IET Microwaves, Antennas & Propagation*, vol. 10, no. 2, pp. 208-214, 2016.

[27] P. Rocca, R. J. Mailloux, and G. Toso, "GA-Based optimization of irregular sub-array layouts for wideband phased arrays desig," *IEEE Antennas and Wireless Propag. Lett.*, vol. 14, pp. 131-134, 2015.

[28] P. Rocca, M. Donelli, G. Oliveri, F. Viani, and A. Massa, "Reconfigurable sum-difference pattern by means of parasitic elements for forward-looking monopulse radar," *IET Radar, Sonar & Navigation*, vol 7, no. 7, pp. 747-754, 2013.

[29] P. Rocca, L. Manica, and A. Massa, "Ant colony based hybrid approach for optimal compromise sum-difference patterns synthesis," *Microwave Opt. Technol. Lett.*, vol. 52, no. 1, pp. 128-132, Jan. 2010.

[30] P. Rocca, L. Manica, and A. Massa, "An improved excitation matching method based on an ant colony optimization for suboptimal-free clustering in sum-difference compromise synthesis," *IEEE Trans. Antennas Propag.*, vol. 57, no. 8, pp. 2297-2306, Aug. 2009.

[31] N. Anselmi, L. Poli, P. Rocca, and A. Massa, "Design of simplified array layouts for preliminary experimental testing and validation of large AESAs," *IEEE Trans. Antennas Propag.*, vol. 66, no. 12, pp. 6906-6920, Dec. 2018.

[32] M. Salucci, F. Robol, N. Anselmi, M. A. Hannan, P. Rocca, G. Oliveri, M. Donelli, and A. Massa, "S-Band spline-shaped aperture-stacked patch antenna for air traffic control applications," *IEEE Trans. Antennas Propag.*, vol. 66, no. 8, pp. 4292-4297, Aug. 2018.

[33] F. Viani, F. Robol, M. Salucci, and R. Azaro, "Automatic EMI filter design through particle swarm optimization," *IEEE Trans. Electromagnet. Compat.*, vol. 59, no. 4, pp. 1079-1094, Aug. 2017.